IEEE Access
Multidisciplinary | Rapid Review | Open Access Journal

Received 8 July 2023, accepted 23 July 2023, date of publication 25 July 2023, date of current version 8 August 2023.

Digital Object Identifier 10.1109/ACCESS.2023.3298874

RESEARCH ARTICLE

T-Type Modular DC Circuit Breaker (T-Breaker) as a Compensator for Future DC Grids

FAISAL ALSAIF[1], (Student Member, IEEE), YUE ZHANG[2], (Student Member, IEEE), XIAO LI[2], (Student Member, IEEE), NIHANTH ADINA[2], (Student Member, IEEE), KHALID ALKHALID[1], (Student Member, IEEE), AND JIN WANG[2], (Fellow, IEEE)

[1]Department of Electrical Engineering, College of Engineering, King Saud University, Riyadh 11421, Saudi Arabia
[2]Department of Electrical and Computer Engineering, College of Engineering, The Ohio State University, Columbus, OH 43210, USA

Corresponding author: Faisal Alsaif (faalsaif@ksu.edu.sa)

This work is based upon research supported by The Advanced Research Projects Agency-Energy (ARPA-E) under award number DE-AR0001110. The authors extend their appreciation to the Deputyship for Research and Innovation, "Ministry of Education" in Saudi Arabia for funding this research (IFKSUOR3-262-2).

ABSTRACT When ac and dc microgrids get exposed to load power changes or voltage transients, instability could occur owing to constant power loads' (CPLs) behaviour. CPL has the negative impedance behaviour which is the reason behind such instability. A flexible alternating current transmission system (FACTS) devices are used in ac grid to help improve the power quality under such circumstances. Contrarily, dc networks doesn't have such devices and suffers under similar situations. In this paper, the T-Type Modular Dc Circuit Breaker (T-Breaker) is proposed to act as a compensator device for dc networks when energy storage is integrated. Its compensation functions in addition to breaking and limiting a system's current can be achieved using this single device. By implementing the T-Breaker's shunt (current) and series (voltage) compensations, ride-through of grid transients can be achieved. T-Breaker's series compensation function and how it can be integrated with the shunt compensation to improve the stability of a dc microgrid is the focus in this paper. In addition to modeling and simulating the system, both small signal and large signal stability are analyzed. Furthermore, a scaled down 270 V 5 kW system is utilized to validate T-Breake's compensation functions and their influence on a microgrid's stability.

INDEX TERMS T-Breaker, series compensation, series-shunt compensation, DC microgrid, constant power load, solid state circuit breaker, Silicon Carbide (SiC).

I. INTRODUCTION

Developments in power electronics allowed dc microgrids becoming a common choice of power distribution option for applications like data centers, commercial buildings [1], vehicles on land, air or sea [2], [3], [4], [5]. When a load changes suddenly or a fault occurs in a microgrid, the microgrid's dc bus voltage can fluctuate. Such transients in the bus voltage can negatively affect the power quality of the microgrid [6]. Due to the negative impedance behavior of Constant Power Loads (CPLs), dc networks could become unstable when there is a significant bus voltage transient. Stability concerns of dc networks containing CPL have been explored in literature [7], [8], [9], [10], [11].

The associate editor coordinating the review of this manuscript and approving it for publication was Yuh-Shyan Hwang.

Literature has introduced many solutions to surmount the instability of CPLs. First approach to assure dc microgrid's stability is to modify passive components [9]. However, heavy capacitors or inductors will reduce the power density in vehicular applications (ships, aviation…etc) where minimized weight and size are targeted. Second, overcoming these transients can be achieved by controlling the source or load side converters. [7], [12], [13], [14], [15], [16]. This approach cannot be generalized because it can only be built for a particular converter. To enhance stability, the third option recommends adding an auxiliary circuit on the load side and utilizing energy storage to alter the corresponding impedance of the CPL [11], [17]. Voltage compensation is the suggested approch in this study, where voltage inserting/absorbing is introduced to enhance system's reliability by sustaining CPL's input voltage during bus voltage transients.

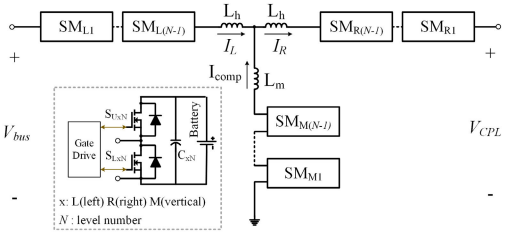

FIGURE 1. T-Breaker's generic system diagram using half bridge submodules.

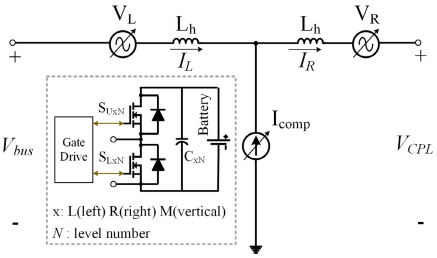

FIGURE 2. T-Breaker equivalent circuit in Series-Shunt compensation mode.

Voltage compensation will be accomplished using the recently developed T-Type Modular Dc Circuit Breaker (T-Breaker) [18], [19].

T-Breaker utilization in a microgrid aids the achievement of protection and compensation tasks Fig.1 depicts the schematic of a generic T-breaker system. The modular structure design of the T-Breaker's allows it to be used in low and medium voltage microgrids. When energy storage devices are integrated across its arms, it can accomplish the compensation tasks. When controlling T-Breaker's vertical arm's submodules, shunt (current) injection/absorption can be achieved [20]. When the two horizontal arms' submodules are controlled, series (voltage) insertion/absorption can be realized. When these two compensation functions are implemented, the T-Breaker can resemble the flexible alternating current transmission system (FACTs) devices in ac networks [21]. T-Breaker being used as all-in-one device which can clear fault current [18], [19] and compensates against voltage and current disturbances can change and improve the landscape of dc networks. A brief discussion of the T-Breaker's breaking function [18] as well as the shunt compensation alone are presented here. The principle, operation, control and analysis of the series and series-shunt compensation functions utilizing the T-Breaker hardware are the main contribution of this work and they are thoroughly studied. Where large signal analysis, small signal analysis, and simulation of the modelled system are shown. In addition, an experimental results of a scaled down dc microgrid is presented for validation of the T-Breaker's compensation functions.

II. T-BREAKER'S BREAKING FUNCTION

T-Breaker is derived based on the modular multilevel converter concept [18]. It has three arms: left arm, right arm and vertical arm. Each arm can be formed by multiple half-bridge or full-bridge submodules connected in series. By controlling the switching of submodule devices, submodules can be represented as controllable voltage sources or current sources as shown in Fig.2. T-Breaker is supposed to operate in the normal operation mode unless there's a fault in the system.

In the normal operation mode, the power from source is directly delivered to the load. All the horizontal submodules are in the bypass state and the equivalent voltages of V_L and V_R are zero. The submodules in the vertical arm are in the off state and the magnitude of I_{comp} is zero.

The breaking mode is triggered when a high current fault is detected. During the breaking mode, all the switches in horizontal submodules are off. The fault current will flow through the anti-parallel diodes into submodules' capacitors as shown in Fig.3. The fault energy will be absorbed by the submodules' capacitors and fault current will decrease to zero. In the meanwhile, submodules in the vertical arm are in the off state; I_{comp} is zero.

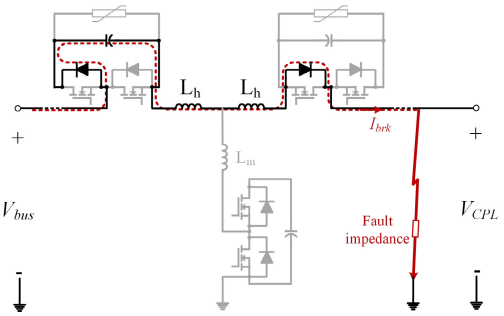

FIGURE 3. T-Breaker equivalent circuit in breaking operation mode.

A 1-kV, 500-A, 3-level half-bridge proof-of-concept T-Breaker prototype was developed and system tests were performed to verify the proposed operation of the T-Breaker [19]. The specifications are listed in Table. 1.

TABLE 1. System & T-Breaker prototype specification.

Parameter	Variable	Value
Dc bus voltage	V_{dc}	1 kV
Nominal dc current	I_{nom}	500 A
Efficiency		99.58%
Number of levels	N	3
Sub-module structure		Half Bridge
Horizontal arm SM nominal voltage	$V_{sub,nom}$	500 V

The system level breaking tests are carried out to show the fault current breaking triggered by two different criteria: 1) the current sensor + controller trigger set based on the I^2t characteristics; 2) the maximum allowable current set by the gate drive overcurrent protection circuit. In this test, the cable inductance (1.56 μH) is used as the fault loop inductance. In Fig.4, the breaking test is carried out at 150-V dc bus, and the system responded to the fault based on the current sensor feedback when the fault current developed to 2.22 kA.

[150 V, 2.22 kA, current sensor + controller trigger.]

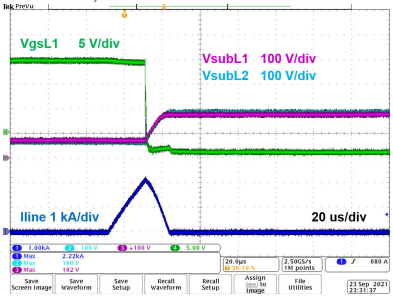

[85 V, 4.24 kA, gate drive overcurrent protection trigger.]

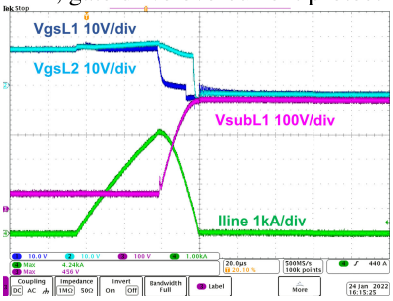

FIGURE 4. System level breaking test waveforms.

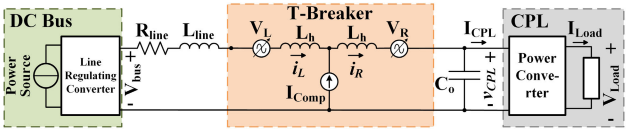

FIGURE 5. Implementation of a T-Breaker in a subsection of dc microgrid.

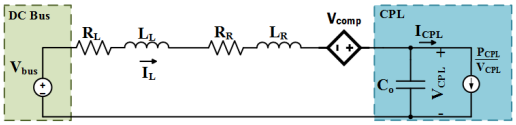

FIGURE 6. SISO dc microgrid having the simplified T-Breaker model as a series compensator.

In Fig.4, the test is carried out at 85-V dc bus. The first submodule (SM_{L1}) on the left arm first detected the overcurrent condition at 4.24 kA before the whole system enters the breaking mode.

III. T-BREAKER'S SERIES COMPENSATION

While the T-Breaker can be installed in any dc microgrid, a dc microgrid subsection that has single-source single-load (SISO) is considered as depicted in Fig.5 to simplify the analysis and the experimental validation. While the switches of the vertical arm are turned off ($I_{comp} = 0$), the voltage compensation is achieved using right arm. Fig.6 is used to present the simplified circuit.

Where left arm resistance R_h and the line resistance R_{line} are combined together and represented as R_L. Left arm inductance L_h and the line inductance L_{line} are combined together

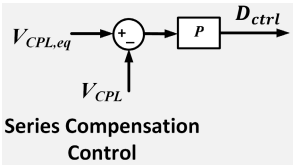

FIGURE 7. Control of the series (voltage) compensation.

and expressed as L_L. The resistance of the right arm is R_R. The inductance of the right arm is L_R.

As illustrated in Fig.7, a simple P control is used to produce compensation voltage (V_{comp}). Thus, V_{comp} is:

$$V_{comp} = K_p * [V_{CPL(ref)} - v_{CPL}]. \tag{1}$$

To realize the state space representation of the system, description of The system is:

$$\begin{aligned} \dot{x}_1 &= -\frac{R_L + R_R}{L_L + L_R} x_1 - \frac{(1 + K_p)}{L_L + L_R} x_2 + \frac{V_{bus}}{L_L + L_R} \\ \dot{x}_2 &= \frac{x_1}{C_o} - \frac{P_{CPL}}{C_o x_2} \end{aligned} \tag{2}$$

where line current i_L is represented by the state variable x_1 and v_{CPL} is represented the state variable x_2. The input voltage is V_{bus} and P_{CPL} is assumed constant. The CPL causes the non-linearity observed in the term $\frac{P_{CPL}}{C_o x_2}$.

The system in (2) needs to be linearized around its equilibrium point X_0 (X_{10}, X_{20}) to examine its small signal stability. Where (3) and (4) show the system after its being linearized. When (4) is used, the system's poles can be located.

$$\begin{bmatrix} \triangle \dot{x}_1 \\ \triangle \dot{x}_2 \end{bmatrix} = A * \begin{bmatrix} \triangle x_1 \\ \triangle x_2 \end{bmatrix} + \begin{bmatrix} \frac{1}{L_L + L_R} \\ 0 \end{bmatrix} * [\triangle U] \tag{3}$$

$$A = \begin{bmatrix} -\frac{R_L + R_R}{L_L + L_R} & -\frac{(1 + K_p)}{L_L + L_R} \\ \frac{1}{C_O} & \frac{P_{CPL}}{C_O * X_{20}^2} \end{bmatrix} \tag{4}$$

The system's large signal stability can be estimated using the region of attraction (ROA) technique. The ROA can be calculated using Takagi-Sugeno (T-S) fuzzy model method [22] which has the advantage of being mathematically valid even in a multi-source multi-load microgrid. Before the disturbance develops, the system needs to be formatted around its equilibrium point using the (T-S) fuzzy model. The new description of the system is:

$$\begin{aligned} \dot{\tilde{x}}_1 &= -\frac{(R_L + R_R)\tilde{x}_1}{(L_L + L_R)} - \frac{(1 + K_p)\tilde{x}_2}{L_L + L_R} \\ \dot{\tilde{x}}_2 &= \frac{1}{C_o}\tilde{x}_1 - \frac{1}{C_o}\tilde{f}\tilde{x}_2 \end{aligned} \tag{5}$$

where $x = (x_1, x_2)$ and $\tilde{x} = x - X_o$

$$\tilde{f} \triangleq \frac{P_{CPL}}{X_{20}} \frac{1}{\tilde{x}_2 + X_{20}}. \tag{6}$$

Because there is only one CPL in this system, two linear equations can be specified as $\dot{\tilde{x}} = A_{LS,i}\,\tilde{x}$ $(i = 1, 2)$ based

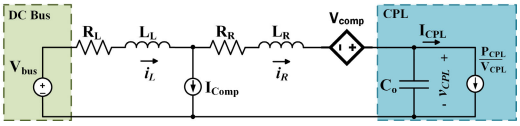

FIGURE 8. SISO dc microgrid having the simplified T-Breaker model as a series-shunt compensator.

on (5). To depict the minimum and the maximum of $\tilde{f}$, $A_{LS,i}$ matrices are utilized as:

$$A_{LS,1} = \begin{bmatrix} -\dfrac{(R_L + R_R)}{(L_L + L_R)} & -\dfrac{1 + K_p}{(L_L + L_R)} \\ \dfrac{1}{C_o} & \dfrac{1}{C_o}\tilde{f}_{min} \end{bmatrix} \tag{7}$$

$$A_{LS,2} = \begin{bmatrix} -\dfrac{(R_L + R_R)}{(L_L + L_R)} & -\dfrac{1 + K_p}{(L_L + L_R)} \\ \dfrac{1}{C_o} & \dfrac{1}{C_o}\tilde{f}_{max} \end{bmatrix}. \tag{8}$$

With the $A_{LS,i}$ matrices, system's stability can be studied by investigating the feasibility of the following Linear Matrix Inequality (LMI):

$$\begin{aligned} P &> 0 \\ A_{LS,i}^T P + P A_{LS,i} &< 0 \quad for \;\; i = 1, 2 \end{aligned} \tag{9}$$

where P is a variable ($P = P^T$) that is needed to satisfy (9).

IV. T-BREAKER'S SERIES-SHUNT COMPENSATION

T-Breaker is used again in the same SISO dc microgrid as illustrated in Fig.5. In this section, switches of the vertical arm are not off anymore ($I_{comp} \neq 0$). Furthermore, the voltage compensation is still achieved using the right arm. The simplified new system circuit is depicted in Fig.8. The contribution here is to make sure that the T-Breaker can realize both compensation function at the same time. However, in real life application it will depend on the state of charge (SoC) of the energy storage units that are connected to each arm. If all arms have high SoC, they can simultaneously compensate. Else, the arms with low SoC will not be required to contribute.

Compensation voltage (V_{comp}) is generated using the same P control as presented in Fig.7. While the current to be compensated follows the Smart Resistor control [11] which ensures the smooth transition from the original operating point to the new operating point as illustrated in Fig.9. Shunt arm's reference current is generated from the Smart Resistor control part. The duty cycle (D_{ctrl}) is then generated by the compensation circuit control part to trace the shunt arm's current. When the circuit is exposed to any disruption, such as a change in source voltage/load power, V_{CPL} or I_R will change I_{comp} as illustrated in (10). The system attempts to maintain system stability by adhering to the relationship defined by the Smart Resistor control. Thus, the two crucial gains (R_{SR} and k_p) which can impact the operation and overall stability are included in the control algorithm. Where the Smart Resistor's slope is controlled by the R_{SR} gain.

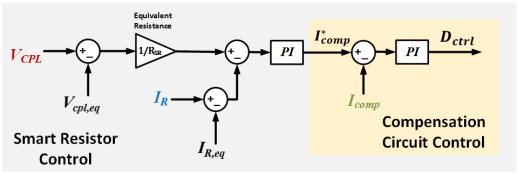

FIGURE 9. Shunt (current) compensation control.

While the tracking speed of I_{comp} is controlled using the k_p gain. Hence, to achieve a resistive total impedance formed by the T-Breaker and the CPL, the reference for the vertical arm's compensating current I_{comp} can be produced. The introduction of $I_{R,eq}$; $V_{cpl,eq}$ terms is to guarantee that when the system is at equilibrium $I_{comp} = 0$. Since the control relies on traditional state machines and PI controllers to realize the Smart Resistor control, the computational efforts aren't high. As highlighted in [14], the SR is essentially an outer loop controller for the system.

Hence V_{comp} and I_{comp} can be defined as:

$$\begin{aligned} V_{comp} &= K_{pv} * [V_{cpl(ref)} - v_{cpl}] \;\; and \\ I_{comp} &= K_p[(\frac{v_{CPL} - V_{CPL,eq}}{R_{SR}}) + (I_{R,eq} - i_R)] \end{aligned} \tag{10}$$

where K_{pv} represent the PI controller for gain for the series compensation while K_p and R_{SR} are the parameters that will define the Smart Resistor's I_{comp} response. Increasing K_p and reducing R_{SR} will result in higher bandwidth requirements and more energy consumption [11]. The new system can be described as:

$$\begin{aligned} \dot{x}_1 &= -\frac{M}{N}x_1 - \frac{J}{N}x_2 + \frac{L_L K_p}{N * C_o R_{SR}}\frac{P_{CPL}}{x_2} + \frac{V_{bus}}{N} \\ \dot{x}_2 &= \frac{x_1}{C_o} - \frac{P_{CPL}}{C_o x_2} \end{aligned} \tag{11}$$

where:

$$\begin{aligned} N &= L_L(1 - Kp) + L_R \\ M &= R_L(1 - Kp) + R_R + \frac{L_L Kp}{C_o R_{SR}} \\ J &= (1 + K_{pv}) + \frac{R_L K_p}{R_{SR}}. \end{aligned}$$

State variables follow the previous definition, where line current i_L is represented by the state variable x_1 and v_{CPL} is represented the state variable x_2. V_{bus} is the input and P_{CPL} is assumed constant.

The equilibrium point X_0, (X_{10}, X_{20}) is used in the linearization of the system in (11) around it and small signal stability of the system can then be investigated. (12) and (13) below represent the system after its being linearized around its equilibrium point. Utilizing (13), the system's poles locations can be found.

$$\begin{bmatrix} \triangle\dot{x}_1 \\ \triangle\dot{x}_2 \end{bmatrix} = A_{SerShu} * \begin{bmatrix} \triangle x_1 \\ \triangle x_2 \end{bmatrix} + \begin{bmatrix} \frac{1}{L_L + L_R} \\ 0 \end{bmatrix} * [\triangle U] \tag{12}$$

TABLE 2. System parameters.

Parameter	Variable	Value
Voltage of the dc bus	V_{bus}	400 V
CPL power	P_{CPL}	50 kW
Line resistance	R_{line}	100 mΩ
Line inductance	L_{line}	100 μH
Horizontal arm resistance of the T-Breaker	R_h	1 mΩ each
Horizontal arm inductance of the T-Breaker	L_h	2 μH each
Submodule capacitance	C_x	65 μF
CPL bus capacitance	C_o	0.25 mF

$$A_{SerShu} = \begin{bmatrix} -\frac{M}{N} & -\frac{1}{N}[(1+K_{pv}) + \frac{R_L Kp}{R_{SR}} - \frac{L_L K_p}{C_o R_{SR}} \frac{P_{CPL}}{X_{20}^2}] \\ \frac{1}{C_o} & \frac{P_{CPL}}{C_o * X_{20}^2} \end{bmatrix} \tag{13}$$

Similar to the previous section, ROA technique is utilized to investigate the system's large signal stability where the (T-S) fuzzy model is realized and the system is described as:

$$\begin{aligned} \dot{\tilde{x}}_1 &= -\frac{M}{N}\tilde{x}_1 - \frac{(J+M\tilde{f})}{N}\tilde{x}_2 \\ \dot{\tilde{x}}_2 &= \frac{1}{C_o}\tilde{x}_1 + \frac{1}{C_o}\tilde{f}\tilde{x}_2 \end{aligned} \tag{14}$$

where $x = (x_1, x_2)$ and $\tilde{x} = x - X_o$ and

$$\tilde{f} \triangleq \frac{P_{CPL}}{X_{20}} \frac{1}{\tilde{x}_2 + X_{20}}. \tag{15}$$

Because there is still only one CPL in this system, two linear equations can be specified as $\dot{\tilde{x}} = A_{SerShu-LS,i}\,\tilde{x}$ $(i = 1, 2)$ based on (5). To depict the minimum and the maximum of $\tilde{f}$, $A_{SerShu-LS,i}$ matrices are utilized as:

$$A_{SerShu-LS,1} = \begin{bmatrix} -\frac{M}{N} & -\frac{1}{N}[J + M\tilde{f}_{min})] \\ \frac{1}{C_o} & \frac{1}{C_o}\tilde{f}_{min} \end{bmatrix} \tag{16}$$

$$A_{SerShu-LS,2} = \begin{bmatrix} -\frac{M}{N} & -\frac{1}{N}[J + M\tilde{f}_{max}] \\ \frac{1}{C_o} & \frac{1}{C_o}\tilde{f}_{max} \end{bmatrix} \tag{17}$$

and the same analysis steps are carried out again.

V. CASE STUDY

A typical motor drive load [10] operating in a constant power mode in a distribution dc network is taken into consideration to examine the small signal stability and the large signal stability of a simplified (SISO) dc microgrid structure. The influence of both compensation functions on the stability of that system is examined. The chosen system's parameters are shown in Table 2.

A. SERIES COMPENSATION

The vicinity of the system's equilibrium point X_0 is used to analyze the small signal stability. When examining the system's poles location, the small signal stability is revealed in Fig.10. Utilizing a small load side capacitor $C_o = 0.25\,mF$ leads to an unstable system due to the fact that the poles are located in the right hand side of the plane. The influence of the C_o capacitor's size on the stability is shown in the same figure,too. The system became stable and the stability can be improved further by having larger capacitance. Though this is a simple approach that enhanced the system's stability, the system's size and weight will increase which is often undesired. On the other hand, the impact of utilizing the series compensation function on improving the system's stability is depicted in Fig.11. it can be observed that when keeping the same CPL capacitance C_o at 0.25 mF ($K_p = 2$), T-Breaker's series (voltage) compensation ensured system's stability.

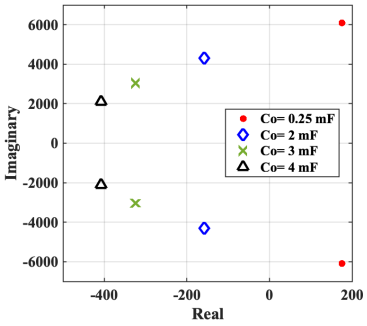

FIGURE 10. Effect of C_o on the small signal stability.

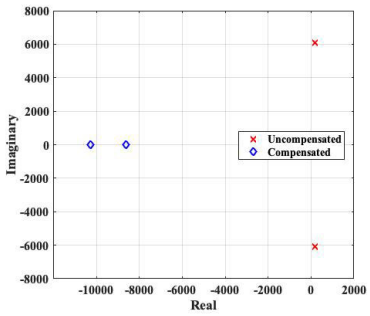

FIGURE 11. Effect of compensation on the small signal stability.

Large signal stability of the system is also examined to observe the influence of the series compensation. To estimate the system's ROA, Matrices (7), (8) are utilized. Fig.12 shows that utilizing $C_o = 0.25\,mF$ without compensation revealed a system with no ROA (unstable). However, the ROA started to exist and kept increasing as the CPL capacitance increases. Contrarily, system with compensation displays a ROA when the initial 0.25-mF Co is maintained as illustrated in Fig.13 ($K_p = 1$, $R_{SR} = 0.1$ $p.u.$). Fig.14 illustrates the large signal analysis in Simulink when using the switching model. It can be seen that under a 10 % source voltage sag, the compensation is able to stabilize the system ($K_p = 1$).

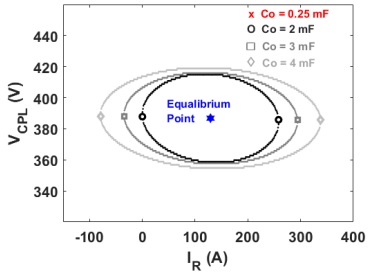

FIGURE 12. Uncompensated system's ROA.

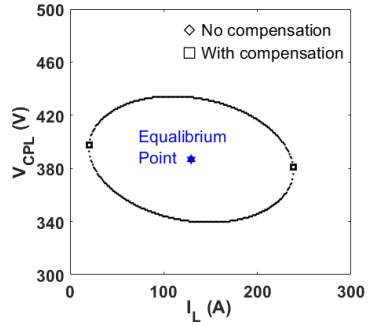

FIGURE 13. Compensated system's ROA.

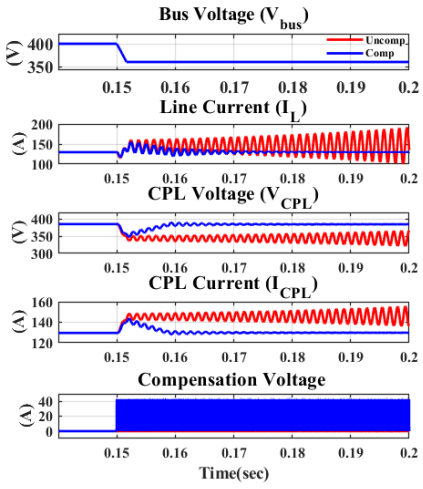

FIGURE 14. Response of the simulated system with and without the series compensation to a 10 % source voltage sag.

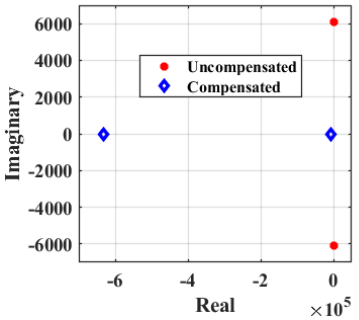

FIGURE 15. Small signal stability: effect of series-shunt compensation.

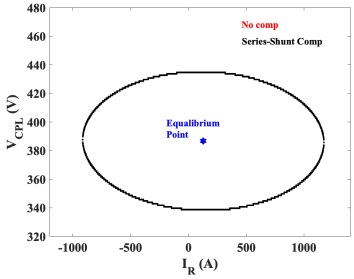

FIGURE 16. ROA of series-shunt compensated system ($K_p = 1$, $R_{SR} = 0.1\ p.u.$).

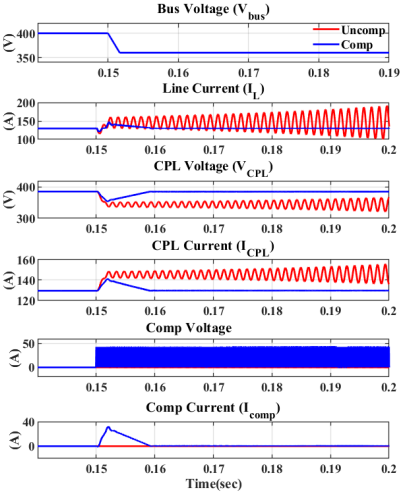

FIGURE 17. Response of the simulated system with and without the series-shunt compensation to a 10 % source voltage sag.

B. SERIES-SHUNT COMPENSATION

When both compensations are enabled, vertical arm's current and horizontal arm's voltage are injectd during a bus votage sag. The system's small signal stability is investigated around its equilibrium point X_0. system's small signal stability without compensation and under the influence of the load side capacitance is similar to what is shown in Fig.10. Fig.15 depicts how the compensation improved the stability. It shows that the series-shunt compensation has pushed the poles that are in the left side of the imaginary axis further, hence, the system is more stable. The series-shunt compensation of the T-Breaker allowed the system to become stable while the CPL capacitance C_o is kept at 0.25 mF ($K_p = 2$).

Large signal stability of the system with and without the series-shunt compensation are assessed. To approximate the system's ROA, matrices (7), (8) are utilized. Fig.16 has no red circle to present the ROA which indicate the unstability of the uncompensated system at $C_o = 0.25\ mF$. Contrarily, the black circle representing the ROA of the compensated system confirms the stability of the compensated system while maintaining the same C_o. Similarly, Fig.17 illustrates the large signal analysis in Simulink when using the switching model.

TABLE 3. Scaled-down system parameters.

Parameter	Variable	Value
Voltage of the dc bus	V_{bus}	270 V
CPL power	P_{CPL}	5 kW
Line resistance	R_{line}	10 mΩ
Line inductance	L_{line}	65 μH
Horizontal arm resistance of the T-Breaker	R_h	1 mΩ
Horizontal arm inductance of the T-Breaker	L_h	2 μH
Submodule capacitance	C_x	65 μF
CPL capacitance	C_o	220 μF
Submodules' switching frequency	f_{sw}	40 kHz

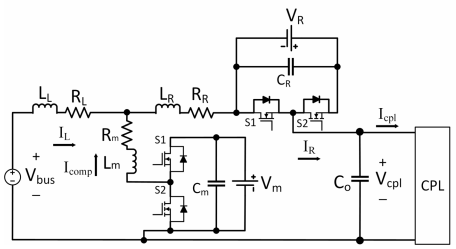

FIGURE 18. Scaled-down hardware test circuit.

It can be seen that under a 10 % source voltage sag, the compensation is able to stabilize the system ($K_p = 1$). The shunt (current) compensation operated only in the beginning to ensure the smooth transition after the disturbance occurred, and once the right arm's voltage injection brought the CPL voltage back to its original value the current went back to zero. Hence, having both compensation functioning together brought the advantage of stabilizing the system and bringing the CPL voltage back to its operating point. In real life application, the standardized grid sag should not last more than 40 ms which helps when it comes to designing the energy storage. Here, the purpose is to verify the functionality of this new concept while the energy storage requirements should be determined by each application (microgrid's voltage and current levels).

VI. EXPERIMENTAL VERIFICATION

To verify and validate the influence of the presented compensation features on the stability, a scaled down system of a dc microgrid is built while integrating the T-Breaker in it. Fig.18 shows the circuit model of the scaled down system that is built in the lab. Test setup's parameters are shown in Table 3. To maintain V_{bus}, a dc power supply is utilized to emulate an active rectifier that has a constant output voltage. To emulate a CPL, an electronic load is utilized.

Test setup is shown in Fig.19. While the system is normally operating at 270 V and supplying a 5 kW CPL, a (20%) bus voltage drop is introduced. The experiment was conducted twice, once without the compensation and once with the series compensation. Fig.20 has the following waveforms: V_{bus}, I_L, V_{CPL}, I_{CPL} and the compensation voltage $V_{ds(S_{LR})}$ to show the system's uncompensated response. Fig.21 depicts the same waveforms of such system when the series compensation was enabled to maintain the CPL voltage

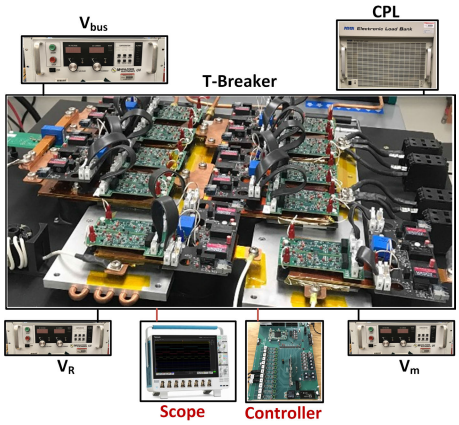

FIGURE 19. Hardware test setup.

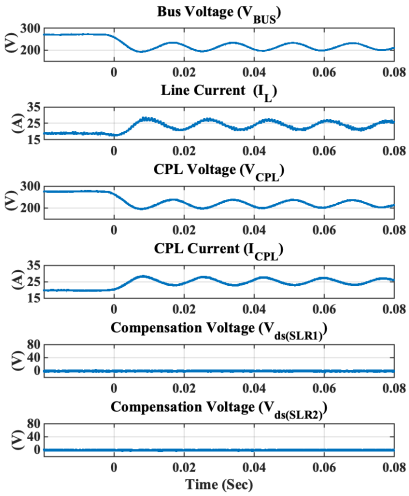

FIGURE 20. Measured uncompensated system response to a 20 % bus voltage sag.

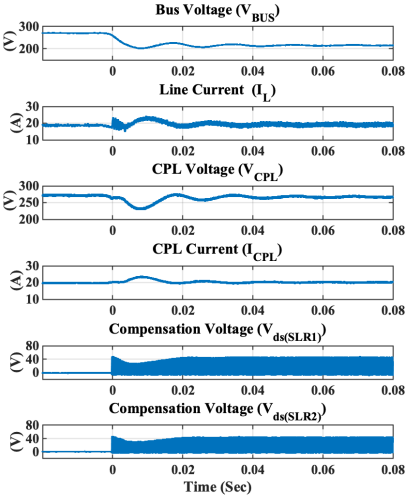

FIGURE 21. Measured system response to a 20 % bus voltage sag using series compensation ($K_p = 1$).

at 270 V. It is noticed that the T-Breaker's horizontal arm was able to inject the needed voltage to help maintaining the load voltage. The stability of the system improved by

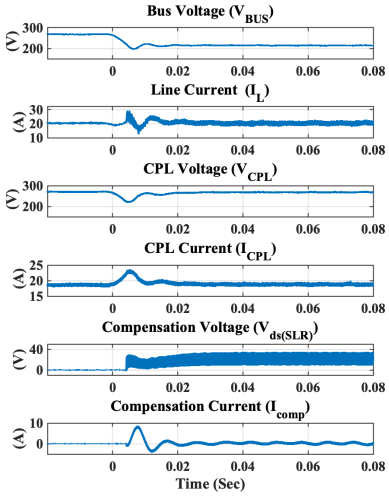

FIGURE 22. Measured system response to a 20 % bus voltage sag using series-shunt compensation together ($K_{pv} = 1$, $K_p = 0.25$, $R_{SR} = 2$.

the compensation where the line current oscillations reduced by 30%. The other experimental result shown in Fig.22 illustrate the impact of using both series and shunt compensation on improving the stability. In this case, the T-Breaker's horizontal arm helped maintaining the CPL voltage while the vertical arm helped with injecting the current needed to achieve the Smart Resistor function when the bus voltage started to drop. As a result, with both compensations the system has seen a 30% reduction in the voltage oscillation. Furthermore, the stress on the source to supply more current was avoided -which negatively affects the stability- by using the vertical arm's current injection.

From the Experimental results provided in this section, the impact of using the series compensation alone and when using series-shunt at the same time is observed and can be compared. Utilizing series compensation alone amended the response of the system by maintaining the CPL voltage after the sag occurred. CPL voltage oscillations (pk-pk) reduced by 30% and settling time was 60 ms. When utilizing the series-shunt compensation the system showed similar CPL voltage oscillations improvement. However, the settling time has improved significantly and it's only 30 ms (50% reduction). Dc microgrid stability has improved when utilizing the compensation functions of the T-Breaker.

VII. CONCLUSION

While the T-Breaker has shown the capability to protect the grid, its capability to achieve both series (voltage) and shunt (current) compensation functions together is achieved here. The T-Breaker's horizontal arms when integrated with energy storage can achieve series compensation. While its vertical arm can achieve the shunt compensation utilizing its integrated energy storage. Small signal stability and large signal stability are evaluated to show the stability improvment of a microgrid when utilizing the T-Breaker's compensation. A down-scaled experimental system (270 V, 5 kW) is built and tested. The bus voltage is exposed to a 20% sag and the system response with and without the compensations after the incident are presented. When series-shunt compensation utilized, 30% reduction in line current oscillation and CPL voltage maintenance are realized and settling time is reduced by 50% compared to series compensation alone. As a result, T-Breaker achieving the compensation functions in addition to its breaking function qualifies it to be an all-in-one device that can improve dc networks' power quality. Future work will focus on improving the response of series compensation in dc grids which suffers from oscillation due to the direct injection of voltage in the line. New submodule topologies for the horizontal arms of the T-Breaker will be investigated in order to enhance the response.

ACKNOWLEDGMENT

This work is based upon research supported by The Advanced Research Projects Agency-Energy (ARPA-E) under award number DE-AR0001110. The authors extend their appreciation to the Deputyship for Research and Innovation, "Ministry of Education" in Saudi Arabia for funding this research (IFKSUOR3-262-2).

REFERENCES

[1] F. Zhang, C. Meng, Y. Yang, C. Sun, C. Ji, Y. Chen, W. Wei, H. Qiu, and G. Yang, "Advantages and challenges of DC microgrid for commercial building a case study from Xiamen University DC microgrid," in *Proc. IEEE 1st Int. Conf. DC Microgrids (ICDCM)*, Jun. 2015, pp. 355–358.

[2] H. Zhang, C. Saudemont, B. Robyns, N. Huttin, and R. Meuret, "Stability analysis on the DC power distribution system of more electric aircraft," in *Proc. 13th Int. Power Electron. Motion Control Conf.*, Sep. 2008, pp. 1523–1528.

[3] A. Griffo and J. Wang, "Large signal stability analysis of 'more electric' aircraft power systems with constant power loads," *IEEE Trans. Aerosp. Electron. Syst.*, vol. 48, no. 1, pp. 477–489, Jan. 2012.

[4] G. Sulligoi, D. Bosich, G. Giadrossi, L. Zhu, M. Cupelli, and A. Monti, "Multiconverter medium voltage DC power systems on ships: Constant-power loads instability solution using linearization via state feedback control," *IEEE Trans. Smart Grid*, vol. 5, no. 5, pp. 2543–2552, Sep. 2014.

[5] M. C. Di Piazza, M. Luna, G. La Tona, M. Pucci, A. Accetta, and A. Pietra, "A new method for selecting the voltage level for an advantageous transition to DC distribution in ships," in *Proc. IEEE Int. Conf. Electr. Syst. Aircr., Railway, Ship Propuls. Road Vehicles Int. Transp. Electrific. Conf. (ESARS-ITEC)*, Nov. 2018, pp. 1–5.

[6] D. Kumar, F. Zare, and A. Ghosh, "DC microgrid technology: System architectures, AC grid interfaces, grounding schemes, power quality, communication networks, applications, and standardizations aspects," *IEEE Access*, vol. 5, pp. 12230–12256, 2017.

[7] A. Kwasinski and C. N. Onwuchekwa, "Dynamic behavior and stabilization of DC microgrids with instantaneous constant-power loads," *IEEE Trans. Power Electron.*, vol. 26, no. 3, pp. 822–834, Mar. 2011.

[8] A. Emadi, A. Khaligh, C. H. Rivetta, and G. A. Williamson, "Constant power loads and negative impedance instability in automotive systems: Definition, modeling, stability, and control of power electronic converters and motor drives," *IEEE Trans. Veh. Technol.*, vol. 55, no. 4, pp. 1112–1125, Jul. 2006.

[9] M. Cespedes, L. Xing, and J. Sun, "Constant-power load system stabilization by passive damping," *IEEE Trans. Power Electron.*, vol. 26, no. 7, pp. 1832–1836, Jul. 2011.

[10] P. Magne, D. Marx, B. Nahid-Mobarakeh, and S. Pierfederici, "Large-signal stabilization of a DC-link supplying a constant power load using a virtual capacitor: Impact on the domain of attraction," *IEEE Trans. Ind. Appl.*, vol. 48, no. 3, pp. 878–887, May 2012.

[11] K. A. Potty, E. Bauer, H. Li, and J. Wang, "Smart resistor: Stabilization of DC microgrids containing constant power loads using high-bandwidth power converters and energy storage," *IEEE Trans. Power Electron.*, vol. 35, no. 1, pp. 957–967, Jan. 2020.

[12] J. Siegers, S. Arrua, and E. Santi, "Stabilizing controller design for multi-bus MVdc distribution systems using a passivity-based stability criterion and positive feedforward control," *IEEE J. Emerg. Sel. Topics Power Electron.*, vol. 5, no. 1, pp. 14–27, Mar. 2017.
[13] H. Farsizadeh, M. Gheisarnejad, M. Mosayebi, M. Rafiei, and M. H. Khooban, "An intelligent and fast controller for DC/DC converter feeding CPL in a DC microgrid," *IEEE Trans. Circuits Syst. II, Exp. Briefs*, vol. 67, no. 6, pp. 1104–1108, Jun. 2020.
[14] Q. Xu, Y. Yan, C. Zhang, T. Dragicevic, and F. Blaabjerg, "An offset-free composite model predictive control strategy for DC/DC buck converter feeding constant power loads," *IEEE Trans. Power Electron.*, vol. 35, no. 5, pp. 5331–5342, May 2020.
[15] C. A. Soriano-Rangel, W. He, F. Mancilla-David, and R. Ortega, "Voltage regulation in buck-boost converters feeding an unknown constant power load: An adaptive passivity-based control," *IEEE Trans. Control Syst. Technol.*, vol. 29, no. 1, pp. 395–402, Jan. 2021.
[16] Y. Gui, R. Han, J. M. Guerrero, J. C. Vasquez, B. Wei, and W. Kim, "Large-signal stability improvement of DC–DC converters in DC microgrid," *IEEE Trans. Energy Convers.*, vol. 36, no. 3, pp. 2534–2544, Sep. 2021.
[17] K.-T. Mok, M.-H. Wang, S.-C. Tan, and S. Y. R. Hui, "DC electric springs—A technology for stabilizing DC power distribution systems," *IEEE Trans. Power Electron.*, vol. 32, no. 2, pp. 1088–1105, Feb. 2017.
[18] Y. Zhang, F. Alsaif, X. Li, R. Na, and J. Wang, "T-type modular DC circuit breaker (T-Breaker) for future DC networks," in *Proc. IEEE Appl. Power Electron. Conf. Expo. (APEC)*, Jun. 2021, pp. 1146–1152.
[19] Y. Zhang, X. Li, D. Ma, Y. Cong, F. Alsaif, Z. Zhang, R. Borjas, B. Hu, J. Wang, B. Riar, J. Ewanchuk, A. Sur, and V. Blasko, "Development of a 1 kV, 500 A, SiC-based T-type modular DC circuit breaker (T-Breaker)," in *Proc. IEEE 8th Workshop Wide Bandgap Power Devices Appl. (WiPDA)*, Nov. 2021, pp. 199–204.
[20] F. Alsaif, Y. Zhang, X. Li, B. Hu, N. Adina, D. Ma, K. Alkhalid, and J. Wang, "Shunt compensation for DC microgrid stabilization utilizing T-type modular DC circuit breaker," in *Proc. IEEE Appl. Power Electron. Conf. Expo. (APEC)*, Mar. 2022, pp. 1538–1542.
[21] F. Z. Peng and J. Wang, "Flexible transmission and resilient distribution systems enabled by power electronics," in *Power Electronics in Renewable Energy Systems and Smart Grid: Technology and Applications*. Hoboken, NJ, USA: Wiley, 2019, pp. 271–314.
[22] L. Herrera, W. Zhang, and J. Wang, "Stability analysis and controller design of DC microgrids with constant power loads," *IEEE Trans. Smart Grid*, vol. 8, no. 2, pp. 881–888, Mar. 2017.

FAISAL ALSAIF (Student Member, IEEE) was born in Riyadh, Saudi Arabia. He received the B.S. degree in electrical and computer engineering from King Saud University, Riyadh, in 2014, and the master's and Ph.D. degrees in electrical engineering from The Ohio State University, Columbus, OH, USA, in 2017 and 2022, respectively.

He is currently an Assistant Professor with King Saud University. His research interests include power and energy, power electronics, high voltage, smart grids, and power quality improvement.

YUE ZHANG (Student Member, IEEE) received the bachelor's degree from Central South University, Changsha, China, and the master's and Ph.D. degrees in electrical engineering from The Ohio State University, Columbus, OH, USA, in 2017 and 2022, respectively.

XIAO LI (Student Member, IEEE) received the B.S. degree in electrical engineering from Shandong University, Jinan, China, in 2015, and the M.S. and Ph.D. degrees in electrical engineering from The Ohio State University, Columbus, OH, USA, in 2017 and 2022, respectively. Her research interests include wide bandgap power semiconductor devices and their applications, including high-frequency, high power density power converters, and circuit breakers.

NIHANTH ADINA (Student Member, IEEE) received the B.Tech. degree in electrical and electronics engineering from the Manipal Institute of Technology, in 2017. He is currently pursuing the Ph.D. degree in electrical engineering with The Ohio State University, Columbus, OH, USA.

KHALID ALKHALID (Student Member, IEEE) received the B.S. degree in electrical and computer engineering from King Saud University, Riyadh, Saudi Arabia, in 2013, and the master's and Ph.D. degrees in electrical engineering from The Ohio State University, Columbus, OH, USA, in 2017 and 2022, respectively.

He is currently an Assistant Professor with King Saud University.

JIN WANG (Fellow, IEEE) received the B.S. degree in electrical engineering from Xi'an Jiaotong University, Xi'an, China, in 1998, the M.S. degree in electrical engineering from Wuhan University, Wuhan, China, in 2001, and the Ph.D. degree in electrical engineering from Michigan State University, East Lansing, MI, USA, in 2005. From 2005 to 2007, he was a Core Power Electronics Engineer with Ford Motor Company, Dearborn, MI, USA. In 2007, he joined The Ohio State University, Columbus, OH, USA, as an Assistant Professor, where he became an Associate Professor, in 2013, and a Full Professor, in 2017. He has authored more than 160 peer-reviewed journals and conference publications and holds eight patents. His current research interests include wide-bandgap power devices and their applications, high-voltage and high-power converter/inverters, the integration of renewable energy sources, and the electrification of transportation. He was a recipient of the IEEE Power Electronics Society Richard M. Bass Young Engineer Award, in 2011, and the National Science Foundations CAREER Award, in 2011. At The Ohio State University, he was a recipient of the Ralph L. Boyer Award for Excellence in Undergraduate Teaching Innovation, in 2012, the Lumley Research Award, in 2013, and the Harrison Faculty Award for Excellence in Engineering Education, in 2017. He was the General Chair of the IEEE Future Energy Challenge, in 2016. He was the Steering Committee Chair of the IEEE Future Energy Challenge, in 2017. He was the Tutorial Co-Chair of the IEEE Applied Power Electronics Conference, in 2019. He initiated and served as the General Chair for the First IEEE Workshop on Wide Bandgap Power Devices and Applications, in 2013. From 2008 to 2014, he was an Associate Editor of the IEEE TRANSACTIONS ON INDUSTRY APPLICATIONS. He is currently an Associate Editor of the IEEE TRANSACTIONS ON POWER ELECTRONICS and the IEEE JOURNAL OF EMERGING AND SELECTED TOPICS IN POWER ELECTRONICS.